

# More Higgses at the LHC and the Electroweak Phase Transition

G. C. Dorsch<sup>1</sup>, S. J. Huber<sup>2</sup>, K. Mimasu<sup>2</sup> and J. M. No<sup>2</sup>

<sup>1</sup> *DESY, Theory Group, Notkestrasse 85, D-22607 Hamburg, Germany*

<sup>2</sup> *Department of Physics and Astronomy, University of Sussex, Brighton BN1 9QH, United Kingdom*

A cosmological first order electroweak phase transition could explain the origin of the cosmic matter-antimatter asymmetry. While it does not occur in the Standard Model, it becomes possible in the presence of a second Higgs doublet. In this context, we obtain the properties of the new scalars  $H_0$ ,  $A_0$  and  $H^\pm$  leading to such a phase transition, showing that its key LHC signature would be the decay  $A_0 \rightarrow H_0 Z$ , and we analyze the promising LHC search prospects for this decay in the  $\ell\ell b\bar{b}$  and  $\ell\ell W^+W^-$  final states. Finally, we comment on the impact of the  $A_0 \rightarrow H_0 Z$  decay on current LHC searches for  $A_0$  decaying into SM particles.

## 1 Introduction

A primary goal of the Large Hadron Collider (LHC) physics programme is the study of the electroweak (EW) symmetry breaking process, its nature and properties. While ATLAS/CMS data from LHC Run 1 have shown that the properties of the discovered Higgs particle are compatible with those expected for the Standard Model (SM) Higgs boson  $h$ , it is possible that the EW symmetry breaking scalar sector includes more states beyond one  $SU(2)_L$  doublet. Extensions of the SM scalar sector such as Two-Higgs-Doublet-Models (2HDMs) could explain the generation of the observed cosmic matter-antimatter asymmetry through EW Baryogenesis<sup>1</sup>. A key requirement for successful baryogenesis is that the EW Phase Transition (EWPT) in the early Universe be strongly first order, which does not occur for the SM with a  $m_h = 125$  GeV Higgs<sup>2</sup>. We show<sup>3</sup> that the primary signature of a strongly first order EWPT in 2HDMs is a large mass splitting  $m_{A_0} - m_{H_0}$ , leading to the decay  $A_0 \rightarrow ZH_0$  as a key LHC probe of such scenario. We then discuss the upcoming LHC prospects in  $\ell\ell b\bar{b}$  and  $\ell\ell W^+W^-$  searches, and comment on the impact of the large mass splitting<sup>4</sup> on current LHC searches for  $A_0/H_0$ .

Altogether, the study in<sup>3</sup> highlights that the decay  $A_0 \rightarrow ZH_0$ , being a ‘smoking gun’ signature of 2HDM scenarios with a strongly first order EWPT, can be probed at the upcoming Run of LHC, thus providing a powerful connection of EW Cosmology to LHC physics.

## 2 The EW Phase Transition with Two Higgs Doublets

The 2HDM scalar sector contains two  $SU(2)_L$  doublet fields  $\Phi_{1,2}$  (see<sup>5,6</sup> for a review of 2HDMs). In addition to the recently observed Higgs boson  $h$ , the 2HDM physical spectrum then contains (in the following we assume for simplicity no Charge-Parity (CP) violation in the scalar sector) another neutral CP-even scalar  $H_0$ , a neutral CP-odd scalar  $A_0$  and a charged scalar  $H^\pm$ . After fixing the EW vacuum expectation value ( $vev$ )  $v = 246$  GeV and the Higgs mass  $m_h = 125$  GeV, the remaining parameters in the scalar potential are: the physical masses  $m_{H_0}$ ,  $m_{A_0}$ ,  $m_{H^\pm}$ , two angles  $\beta$  and  $\alpha$  and a mass scale  $\mu$ . Here  $\alpha$  is defined such that when  $\alpha = \beta$ ,  $h$  has SM-like couplings to gauge bosons and fermions, known as the *alignment limit* (see<sup>7</sup> for details on the 2HDM parameter definitions and conventions used in this work).

Our study of the strength of the EWPT in 2HDMs is performed in a Yukawa Type-I 2HDM. We stress that the Type of 2HDM considered is irrelevant for the EWPT, as the top quark couples to  $\Phi_{1,2}$  in the same way for every 2HDM Yukawa Type scenario. However, experimental constraints do differ among Types<sup>a</sup>. We perform a numerical scan over the parameters  $m_{H_0}$ ,  $m_{A_0}$ ,  $m_{H^\pm}$ ,  $\tan\beta$ ,  $\sin(\alpha - \beta)$  and  $\mu$ , interfaced to 2HDMC<sup>8</sup> and HiggsBounds<sup>9</sup> to select the region

<sup>a</sup>Hence our choice of a Type-I 2HDM (instead of *e.g.* a Type-II 2HDM, for which up-type quarks couple to  $\Phi_2$  while down-type quarks and leptons couple to  $\Phi_1$ ) which is the least constrained one, in order to provide a better gauging of the impact of a first order EWPT on the 2HDM parameter space.

of parameter space that satisfies EW precision constraints and existing collider bounds, as well as theoretical requirements from stability, unitarity and perturbativity. Flavour constraints<sup>10</sup> and constraints from measured Higgs signal strengths on  $\tan\beta$  and  $\sin(\alpha - \beta)$  (see *e.g.*<sup>11</sup>) are also included. Points in our scan satisfying all the above constraints are considered *physical points*. We compute for each of them the strength of the EWPT via the thermal 1-loop effective potential (see<sup>7</sup> for details). The results of our scan are summarized in Figure 1, which shows heat-maps of physical points in the planes  $(m_{H_0}, \alpha - \beta)$  (*left*) and  $(m_{H_0}, m_{A_0})$  (*right*), together with contours for the ratio of strongly first order EWPT points to physical points. A strongly first order EWPT, as needed for successful EW Baryogenesis, is preferentially achieved for a large mass splitting  $m_{A_0} - m_{H_0} \gg m_Z$ , together with a heavy CP-odd scalar  $A_0$  ( $m_{A_0} > 300$  GeV), as shown in Figure 1 (*right*). Such an EWPT also favours an SM-like Higgs  $h$ , *i.e.* small  $\sin(\alpha - \beta)$  and moderate  $\tan\beta$ <sup>3,7</sup>, with the EWPT range in  $\sin(\alpha - \beta)$  shrinking as the state  $H_0$  becomes heavier (see Figure 1 (*left*)).

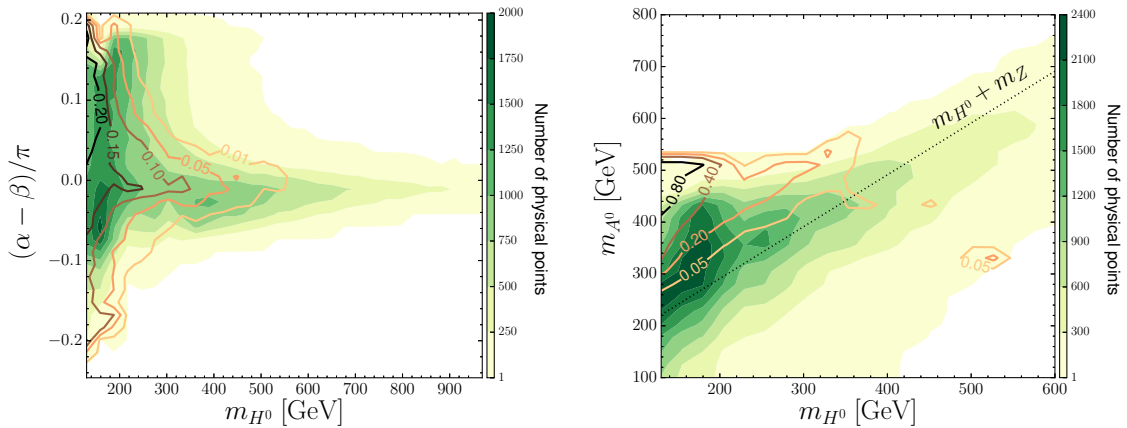


Figure 1 – Heat-maps for physical points in the  $(m_{H_0}, \alpha - \beta)$  (*left*) and  $(m_{H_0}, m_{A_0})$  (*right*) planes. Contours in each case show the region with a certain ratio of strongly first order EWPT points to physical points. The dotted-black line (*right*) corresponds to  $m_{A_0} = m_{H_0} + m_Z$ .

### 3 The Decay Channel $A_0 \rightarrow Z H_0$ and LHC Probes of 2HDM

The large mass splitting  $m_{A_0} - m_{H_0}$  leads to the  $A_0 \rightarrow Z H_0$  decay channel as a characteristic LHC signature of 2HDMs with a strongly first order EWPT. This decay is strongly enhanced both by the large phase space available and by the coupling  $g_{A_0 Z H_0} \sim \cos(\alpha - \beta)$ , unsuppressed in the alignment limit (in contrast with the decay  $A_0 \rightarrow Z h$ , which vanishes in that limit since  $g_{A_0 Z h} \sim \sin(\alpha - \beta)$ ). Regarding competing decay channels,  $A_0 \rightarrow t\bar{t}$  is subdominant for  $m_{A_0} - m_{H_0} > v$ , while the presence of  $A_0 \rightarrow W^\pm H^\mp$  depends on the splitting  $m_{A_0} - m_{H^\pm}$ . EW precision observables require  $H^\pm$  to be close in mass to either  $H_0$  or  $A_0$ <sup>12</sup>, which makes  $A_0 \rightarrow W^\pm H^\mp$  either kinematically forbidden or similar to  $A_0 \rightarrow Z H_0$  (see<sup>3</sup> for a more detailed discussion on these issues). Here we assume for simplicity  $m_{H^\pm} \sim m_{A_0}$ .

In the following we analyze two prototypical scenarios, featuring  $\mu = 100$  GeV,  $\tan\beta = 2$ ,  $m_{A_0} = m_{H^\pm} = 400$  GeV,  $m_{H_0} = 180$  GeV and respectively  $(\alpha - \beta) = 0.001\pi$  (Benchmark A) and  $(\alpha - \beta) = 0.1\pi$  (Benchmark B). These benchmarks characterize the two alternatives for the dominant decay of  $H_0$ :  $H_0 \rightarrow b\bar{b}$  very close to the alignment limit, while away from it  $H_0 \rightarrow W^+ W^-$ . This discussion highlights the fact that for 2HDMs with a strongly first order EWPT, the corresponding “smoking gun” signature at the LHC will either be  $pp \rightarrow A_0 \rightarrow Z H_0 \rightarrow \ell\ell b\bar{b}$  or  $pp \rightarrow A_0 \rightarrow Z H_0 \rightarrow \ell\ell W^+ W^-$ , depending on how close the 2HDM is to the alignment limit.

#### 3.1 LHC Search for $A_0$ in $\ell\ell b\bar{b}$ and $\ell\ell W^+ W^-$

We now analyze the search prospects in the  $\ell\ell b\bar{b}$  and  $\ell\ell W^+ W^-$  channels at the 14 TeV run of the LHC using the defined benchmarks A and B from above. We implement the Type-I 2HDM in FEYNRULES<sup>13</sup> and use MADGRAPH5\_AMC@NLO<sup>14</sup> to generate both signal and

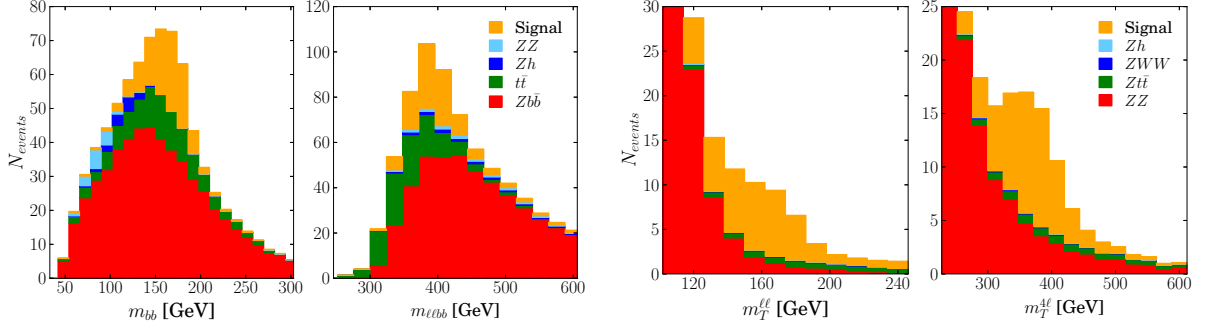


Figure 2 – Left:  $m_{bb}$  (left) and  $m_{\ell\ell bb}$  (right) distributions after analysis cuts, with the various contributions stacked (for  $\mathcal{L} = 20 \text{ fb}^{-1}$ ). Right:  $m_T^{\ell\ell}$  (left) and  $m_T^{4\ell}$  (right) distributions after event selection, with the various contributions stacked (for  $\mathcal{L} = 60 \text{ fb}^{-1}$ ).

background analysis samples, then passed on to PYTHIA<sup>15</sup> and DELPHES<sup>16</sup> for parton showering, hadronization and detector simulation. We first concentrate on Benchmark A, which corresponds to the  $\ell\ell b\bar{b}$  final state. The two main SM backgrounds are: (i)  $Zb\bar{b}$  production (with  $Z \rightarrow \ell\ell$ ), (ii) QCD  $t\bar{t}$  production (with  $t\bar{t} \rightarrow bW^+bW^- \rightarrow b\ell^+\nu_\ell b\bar{\ell}^-\bar{\nu}_\ell$ ). Event selection requires the presence of two isolated same flavour (SF) leptons in the final state with  $P_T^{\ell_1} > 40 \text{ GeV}$ ,  $P_T^{\ell_2} > 20 \text{ GeV}$  and  $|\eta_\ell| < 2.5$  (2.7) for electrons (muons), together with two b-tagged jets in the event with  $P_T^{b_1} > 40 \text{ GeV}$ ,  $P_T^{b_2} > 20 \text{ GeV}$  and  $|\eta_b| < 2.5$ . In order to extract the signal we require  $m_{\ell\ell} = m_Z \pm 10 \text{ GeV}$  and perform the cuts (see<sup>3</sup> for details)  $H_T^{b\bar{b}} > 150 \text{ GeV}$ ,  $H_T^{\ell\ell b\bar{b}} > 280 \text{ GeV}$ ,  $\Delta R_{bb} < 2.5$ ,  $\Delta R_{\ell\ell} < 1.6$ . We define the signal region as  $m_{bb} = (m_{H_0} - 20) \pm 30 \text{ GeV}$  and  $m_{\ell\ell bb} = (m_{A_0} - 20) \pm 40 \text{ GeV}$  and show the  $m_{bb}$  and  $m_{\ell\ell bb}$  distributions after cuts for an integrated luminosity  $\mathcal{L} = 20 \text{ fb}^{-1}$  in Figure 2 (left) (various contributions stacked). A discovery value  $S/\sqrt{S+B} = 5$  ( $S$  = signal events,  $B$  = background events) may be obtained already with  $\mathcal{L} \sim 15 - 20 \text{ fb}^{-1}$  in the limit that only statistical uncertainties are important.

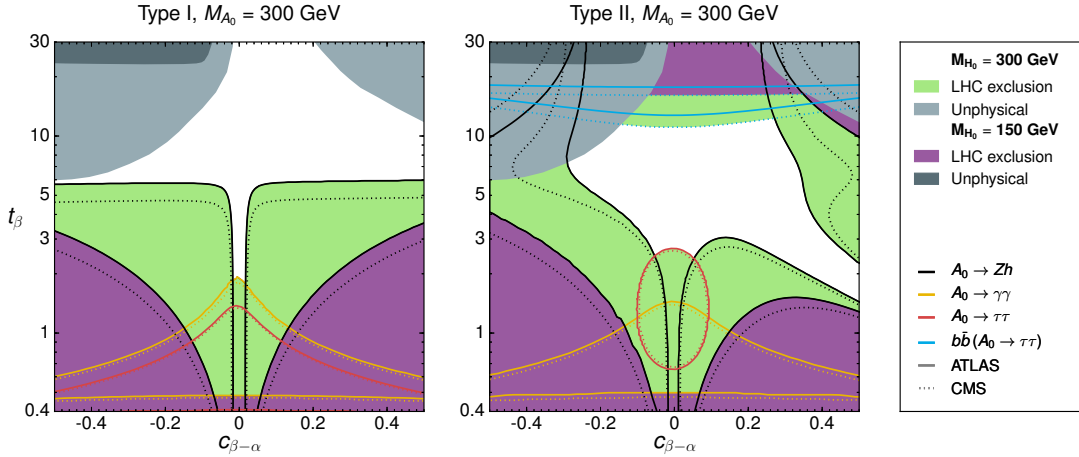


Figure 3 – Current limits in the  $(\sin(\alpha - \beta), \tan\beta)$  plane from ATLAS/CMS searches of  $A_0$  decaying into SM states for 2HDM Type-I (left) and Type-II (right), with  $m_{A_0} = 300 \text{ GeV}$  and  $m_{H_0} = 300 \text{ GeV}$  (light-green exclusion), 150 GeV (purple exclusion) respectively.

Away from alignment (Benchmark B) the decay  $H_0 \rightarrow W^+W^- \rightarrow \ell\nu_\ell\ell\nu_\ell$  (together with  $Z \rightarrow \ell'\ell'$ ) provides the best discovery prospects. The main background is  $ZZ \rightarrow \ell\ell\ell'\ell'$ . For event selection, we require four isolated leptons in the final state with  $P_T^{\ell_1} > 40 \text{ GeV}$ ,  $P_T^{\ell_2, \ell_3, \ell_4} > 20 \text{ GeV}$ , with one SF lepton pair (opposite sign) reconstructing  $m_Z$  within 20 GeV. After event selection, the signal and background cross sections at LHC 14 TeV (at leading order) are respectively 0.93 fb and 5.6 fb. Defining the transverse mass variables  $m_T^{\ell\ell}$  and  $m_T^{4\ell}$

$$\left(m_T^{\ell\ell}\right)^2 = \left(\sqrt{p_{T,\ell\ell}^2 + m_{\ell\ell}^2} + \not{p}_T\right)^2 - (\vec{p}_{T,\ell\ell} + \vec{\not{p}}_T)^2, \quad m_T^{4\ell} = \sqrt{p_{T,\ell'\ell'}^2 + m_{\ell'\ell'}^2} + \sqrt{p_{T,\ell\ell}^2 + m_{\ell\ell}^2} \quad (1)$$

with  $\ell'\ell'$  the two SF leptons most closely reconstructing  $m_Z$ , a signal region of  $m_T^{4\ell} > 260$  GeV (see Figure 2 (*right*)) allows to extract a clean signal<sup>3</sup>. Our final signal cross section is 1.41 fb, which compared to a background of 1.7 fb reaches a significance of 5 with  $\mathcal{L} \sim 60 \text{ fb}^{-1}$ .

### 3.2 Impact of $m_{A_0} - m_{H_0}$ on LHC Searches for $A_0$ into SM States

Finally, we stress that the presence of the dominant decay mode  $A_0 \rightarrow ZH_0$  due to a large splitting  $m_{A_0} - m_{H_0}$  has an important impact on the sensitivity of current searches for  $A_0$  decaying into SM states at the LHC, as the branching fractions into those get significantly reduced for a large mass splitting<sup>4</sup>  $m_{A_0} - m_{H_0}$ . As an example, Figure 3 shows the current limits in the 2HDM parameter plane ( $\sin(\alpha - \beta)$ ,  $\tan\beta$ ) from ATLAS/CMS searches of  $A_0$  decaying into SM states<sup>17</sup>, for  $m_{A_0} = 300$  GeV and  $m_{H_0} = 300$  GeV, 150 GeV respectively, for 2HDM Type-I (*left*) and Type-II (*right*).

### Acknowledgments

S.H. and K.M. are supported by the Science Technology and Facilities Council (STFC) under grant number ST/L000504/1. The work of J.M.N. is supported by the People Programme (Marie Curie Actions) of the European Union Seventh Framework Programme (FP7/2007-2013) under REA grant agreement PIEF-GA-2013-625809.

### References

1. N. Turok and J. Zadrozny, Nucl. Phys. B **358**, 471 (1991); J. M. Cline, K. Kainulainen and A. P. Vischer, Phys. Rev. D **54**, 2451 (1996); L. Fromme, S. J. Huber and M. Seniuch, JHEP **0611** (2006) 038.
2. K. Kajantie, M. Laine, K. Rummukainen and M. E. Shaposhnikov, Phys. Rev. Lett. **77** (1996) 2887.
3. G. C. Dorsch, S. J. Huber, K. Mimasu and J. M. No, Phys. Rev. Lett. **113** (2014) 21, 211802.
4. G. C. Dorsch, S. J. Huber, K. Mimasu and J. M. No, To appear.
5. G. C. Branco, P. M. Ferreira, L. Lavoura, M. N. Rebelo, M. Sher and J. P. Silva, Phys. Rept. **516**, 1 (2012).
6. J. F. Gunion and H. E. Haber, Phys. Rev. D **67** (2003) 075019.
7. G. C. Dorsch, S. J. Huber and J. M. No, JHEP **1310** (2013) 029.
8. D. Eriksson, J. Rathsman and O. Stal, Comput. Phys. Commun. **181**, 189 (2010).
9. P. Bechtle, O. Brein, S. Heinemeyer, O. Stl, T. Stefaniak, G. Weiglein and K. E. Williams, Eur. Phys. J. C **74** (2014) 2693.
10. T. Hermann, M. Misiak and M. Steinhauser, JHEP **1211** (2012) 036.
11. B. Dumont, J. F. Gunion, Y. Jiang and S. Kraml, Phys. Rev. D **90** (2014) 035021; M. Gorbahn, J. M. No and V. Sanz, JHEP **1510** (2015) 036.
12. W. Grimus, L. Lavoura, O. M. Ogreid and P. Osland, J. Phys. G **35**, 075001 (2008); Nucl. Phys. B **801**, 81 (2008).
13. N. D. Christensen and C. Duhr, Comput. Phys. Commun. **180**, 1614 (2009); C. Degrande, C. Duhr, B. Fuks, D. Grellscheid, O. Mattelaer and T. Reiter, Comput. Phys. Commun. **183**, 1201 (2012).
14. J. Alwall, M. Herquet, F. Maltoni, O. Mattelaer and T. Stelzer, JHEP **1106**, 128 (2011); J. Alwall, R. Frederix, S. Frixione *et al.*, JHEP **1407** (2014) 079.
15. T. Sjostrand, S. Mrenna and P. Z. Skands, Comput. Phys. Commun. **178**, 852 (2008).
16. J. de Favereau *et al.* [DELPHES 3 Collaboration], JHEP **1402**, 057 (2014).
17. G. Aad *et al.* [ATLAS Collaboration], Phys. Lett. B **744** (2015) 163; V. Khachatryan *et al.* [CMS Collaboration], Phys. Lett. B **748**, 221 (2015); G. Aad *et al.* [ATLAS Collaboration], Phys. Rev. Lett. **113** (2014) 17, 171801; CMS Collaboration [CMS Collaboration], CMS-PAS-HIG-14-006; G. Aad *et al.* [ATLAS Collaboration], JHEP **1411** (2014) 056; V. Khachatryan *et al.* [CMS Collaboration], JHEP **1410** (2014) 160.